Microchimica Acta (2022) 189: 235
https://doi.org/10.1007/s00604-022-05323-4

ORIGINAL PAPER

3D-printed electrochemical platform with multi-purpose carbon black sensing electrodes

Habdias A. Silva-Neto[1] · Anderson A. Dias[1] · Wendell K. T. Coltro[1,2]

Received: 7 December 2021 / Accepted: 27 April 2022 / Published online: 28 May 2022

Abstract

The 3D printing is described of a complete and portable system comprising a batch injection analysis (BIA) cell and an electrochemical platform with eight sensing electrodes. Both BIA and electrochemical cells were printed within 3.4 h using a multimaterial printer equipped with insulating, flexible, and conductive filaments at cost of ca. ~ U$ 1.2 per unit, and their integration was based on a threadable assembling without commercial component requirements. Printed electrodes were exposed to electrochemical/Fenton pre-treatments to improve the sensitivity. Scanning electron microscopy and electrochemical impedance spectroscopy measurements upon printed materials revealed high-fidelity 3D features (90 to 98%) and fast heterogeneous rate constants ($(1.5 \pm 0.1) \times 10^{-3}$ cm s^{-1}). Operational parameters of BIA cell were optimized using a redox probe composed of $[Fe(CN)_6]^{4-/3-}$ under stirring and the best analytical performance was achieved using a dispensing rate of 9.0 µL s^{-1} and an injection volume of 2.0 µL. The proof of concept of the printed device for bioanalytical applications was evaluated using adrenaline (ADR) as target analyte and its redox activities were carefully evaluated through different voltammetric techniques upon multiple 3D-printed electrodes. The coupling of BIA system with amperometric detection ensured fast responses with well-defined peak width related to the oxidation of ADR applying a potential of 0.4 V *vs* Ag. The fully 3D-printed system provided suitable analytical performance in terms of repeatability and reproducibility (RSD ≤ 6%), linear concentration range (5 to 40 µmol L^{-1}; $R^2 = 0.99$), limit of detection (0.61 µmol L^{-1}), and high analytical frequency (494 ± 13 h^{-1}). Lastly, artificial urine samples were spiked with ADR solutions at three different concentration levels and the obtained recovery values ranged from 87 to 118%, thus demonstrating potentiality for biological fluid analysis. Based on the analytical performance, the complete device fully printed through additive manufacturing technology emerges as powerful, inexpensive, and portable tool for electroanalytical applications involving biologically relevant compounds.

Keywords 3D printing · Fused deposition modeling · Wall-jet cell · Carbon black electrodes · Multiplex system · Adrenaline

Introduction

The technological revolution of digital simulation and computer-aided manufacturing has enabled the popularization of 3D printing [1–3]. Based on the additive manufacturing methods, 3D printing makes possible the construction and customization of objects in a single step [4–6]. One of the most popular 3D printing technologies is known as fused deposition modeling (FDM), which promotes the printing of desirable structures at coordinates previously selected from digital projects in computer-controlled software [7]. 3D-printed objects are created via layer-by-layer deposition of filaments and the device completion time is directly linked to layer thickness and surface finalization. This technology offers very attractive advantages such as low-cost instrumentation, reproduction fidelity, operational simplicity, and possibilities of depositing multiple materials using a wide variety of filaments [8, 9]. In the last years, filaments including materials based on metals, polymers, and carbon with relevant chemical, mechanical, and electrical properties such as low toxicity, flexibility, and conductivity have become commercially available [10–12].

✉ Wendell K. T. Coltro
wendell@ufg.br

[1] Instituto de Química, Universidade Federal de Goiás, Campus Samambaia, Goiânia, GO 74690-900, Brazil

[2] Instituto Nacional de Ciência E Tecnologia de Bioanalítica, Campinas, SP 13084-971, Brazil

Advances in 3D printing technology have contributed to the analytical chemistry including developments from sample preparation to detection [13–18]. Examples of miniaturized devices for solid-phase extraction [19], solution mixing [20], droplet generation [21], mass spectrometry interfacing [22], and analytical separations [23, 24] as well as colorimetric [25] and electrochemical sensors [10] have been successfully reported in the last years. Electrochemical sensors have been by far the most popular analytical tools developed through 3D printing due to low instrumental requirements and satisfactory analytical performance as well as availability of different conductive filaments [11, 12, 16, 26]. Their use in conjunction with flow and bath injection analysis (BIA) enables reproducible injection volumes, low interference involving sample evaporation, efficient surface renovation, multiple sequential analyses, and fast responses [27–29]. When compared to flow injection analysis, BIA systems associated to commercially available electronic micropipettes have ensured better performance once they do not present problems commonly seen in flow-based systems like solution leakage and presence of bubbles [28, 30–32].

Regarding the electrodes often integrated into BIA cells, many studies reported in the literature make use of conventional electrodes [27, 29, 33–35]. Normally, these electrodes are relatively large and bulky, making difficult their use for on-site applications [28, 36, 37]. In 2014, Tormin et al. [38] reported the first study employing screen-printed electrodes (SPE) in the BIA system aiming to minimize the mentioned problems. In their study, the analytical platform was associated to wall-jet approach and the authors successfully demonstrated the electrochemical detection of diclofenac, hydrogen peroxide, and heavy metals.

In the last 5 years, different authors have explored 3D printing to create printed BIA cells [39–41] integrated with commercial [32] or 3D-printed electrodes [40], such as reference (RE), auxiliar (AE), and working (WE) electrodes using filaments composed of acrylonitrile–butadiene–styrene (ABS), polylactic acid (PLA), and PLA doped with carbon black (CB/PLA) or graphene [17, 42]. Recently, Richter et al. [41] designed an interesting architecture including a cell body containing RE, AE, and WE. These printed segments were constructed using a low-cost desktop printer and two filaments (PLA and CB/PLA). The performance of the complete sensing platform was evaluated through voltammetric measurements of dopamine, as a model analyte. However, a non-3D-printed component as a rubber-made O-ring was needed to avoid problems associated with leakage and delimitation of the WE area [41, 43]. Also, to the best of our knowledge, the current state-of-the-art related to 3D-printed electrochemical sensors does not include analytical systems with multiple integrated electrodes.

Here, we report for the first time the fabrication of a 3D-printed BIA cell integrated with multiple sensing electrodes in a single step. The proposed device was fully constructed through a multimaterial desktop printer and its segments were assembled/disassembled through a threading strategy. The 3D-printed cell was integrated with eight CB/PLA electrodes (RE, AE, and WE) and activated through the combination of Fenton degradation followed by electrochemical oxidation, as reported recently [44]. As proof of concept, the integrated electrodes were modified with graphene oxide (GO) and glucose oxidase (GOx). Moreover, multiple electrochemical techniques were explored to evaluate the redox activities of adrenaline (ADR). The sensing platform associated to amperometric detection (BIA-AD) was employed to successfully measure ADR in artificial urine samples. ADR substance is neural and hormonal from catecholamine group. Their presence in the human organism is associated to important biological functions as vasoconstriction, heart rate, and regulator of blood pressure [45–47].

Experimental

Chemicals and materials

Adrenaline, acetic acid, ammonium iron(II) sulfate hexahydrate, boric acid, graphene oxide (GO), glucose oxidase (*Aspergillus niger*, 181 U mg^{-1}) (GOx), hydrochloric acid, hydrogen peroxide, potassium chloride, phosphoric acid, potassium hexacyanoferrate(II) trihydrate, potassium hexacyanoferrate(III), sodium hydroxide, sodium phosphate dibasic, sodium phosphate monobasic, and paracetamol were purchased from Sigma-Aldrich (Saint Louis, MO, USA) and used as received.

Stock and standard solutions were prepared using ultrapure water processed through a water purification system (Direct-Q®3, Millipore, Darmstadt, Germany) with resistivity equal to 18.2 MΩ.cm. Non-conductive thermoplastic filaments (PLA and PLA-flex) were purchased from 3DFila (Belo Horizonte, MG, Brazil). Conductive filament model proto-pasta CB/PLA was received from Protoplant (Vancouver, BC, Canada). A portable LED cabin (7 W) and silver ink pen were purchased from Kiss NY Pro (New York, USA) and MG Chemicals (Burlington, ON, Canada), respectively.

Instrumentation

Electrochemical experiments were realized using a potentiostat/bipotentiostat model μStat 400 from DropSens (Oviedo, Spain) and a PGSTAT-100 N potentiostat from Metrohm-Autolab (Utrecht, Netherlands). The BIA cell was combined with an electronic micropipette model E3 and Combitips® advanced (100 μL) purchased from Eppendorf (Hamburg, Germany). The distance from the electronic micropipette

tip to the electrochemical cell was set at ~ 2 mm [21, 23, 28]. All electrochemical experiments were realized at room temperature (25 ± 2 °C).

3D printing, integration, and activation of sensing electrodes

The BIA cell layout containing eight integrated electrochemical sensors was designed using SolidWorks 2014 software and printed through a multimaterial desktop 3D printer model open-source i3MK2 from Prusa Research (Prague, Czech Republic). Each electrochemical sensor was designed in a conventional three-electrode arrangement including working, reference, and auxiliary electrodes. The design and assembling of individual pieces involved in the fully integrated 3D-printed BIA cell are summarized in Fig. S1, available in the electronic supplementary information (ESI). For the printing process, the STL file was converted into a GCODE file through PrusaSlicer software. The manufacturing method was realized based on the FDM process [10] setting nozzle and bed temperatures at 230 and 60 °C, respectively.

The assembling of the 3D-printed cell segments was based on a threadable strategy, as illustrated in Fig. 1A and Video S1. First, segments I and II are threaded forming the region to insert a micropipette tip. Based on this component, it is possible to select the best distance from the syringe tip to WE. Posteriorly, the parts III, IV, and V are mounted, forming the fully 3D-printed cell integrated with eight electrochemical sensors. It is important to highlight that the segment IV (PLA-flexible) is pressured between parts III and V as a sandwich type, ensuring a reversible sealing.

To select one 3D-printed sensor, the micropipette tip was inserted in the 3D-printed cell and segments (i) and (ii) were then aligned. This mechanism is based on clockwise rotation and allows choosing eight 3D-printed sensors on the same analytical platform (Fig. 1B).

Afterwards, the surfaces of all 3D-printed electrodes were simultaneously polished using a sanding sheet with grit numbers 280 and 1500 impregnated into a 3D-printed piece. The procedure for polishing the electrode surfaces is schematized in Fig. S2 (see ESI).

For improving the electrochemical performance, the surfaces of multiple electrodes were pre-treated through an

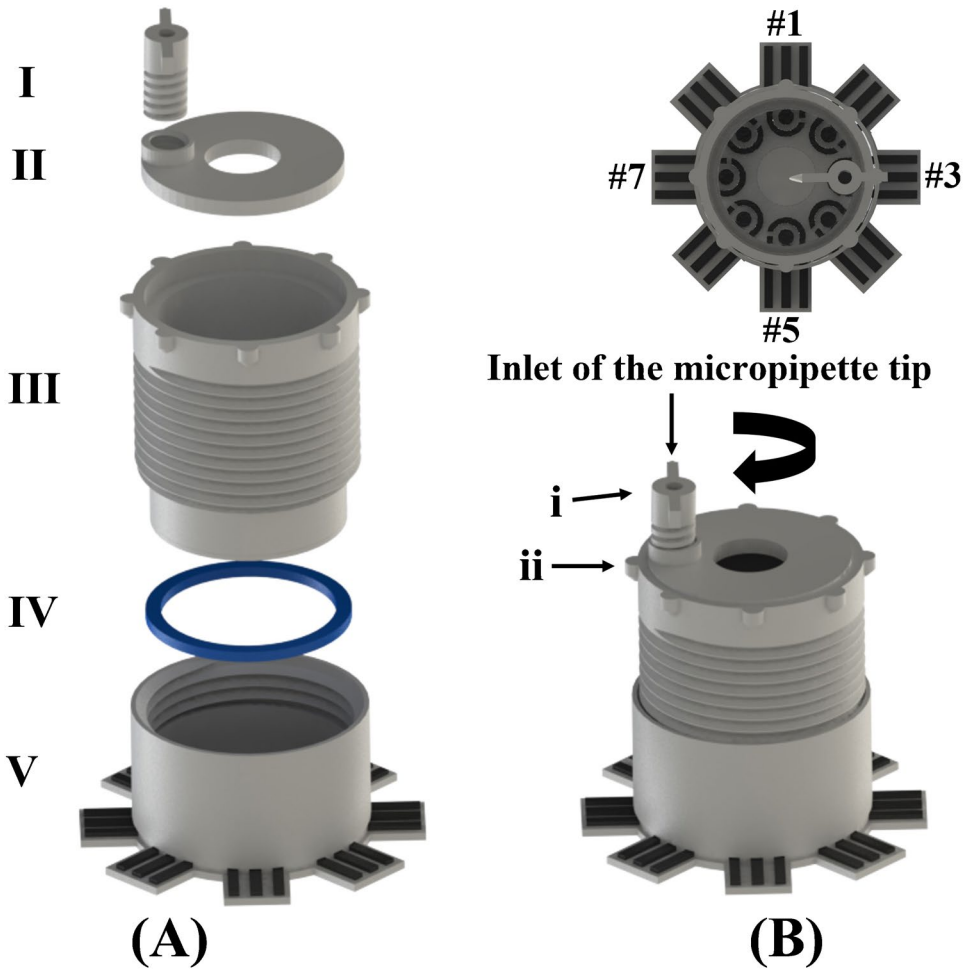

Fig. 1 Scheme showing **A** the assembling of 3D-printed BIA cell with integrated electrodes and **B** the resulting integrated platform. In **A**, the assembling shows (I) micropipette adaptor, (II) top cover, (III) cell body, (IV) flexible printed ring, and (V) cell body with multiple integrated electrodes. In **B**, it is demonstrated a top view of 3D-printed cell and adopted mechanism to select the electrodes based on alignment between parts (i) and (ii)

electrochemical/Fenton method, described elsewhere [44]. Next, reference electrodes were painted with Ag ink, thus creating pseudo-reference electrodes (p-RE), as illustrated in Fig. S3.

Electrochemical measurements using 3D-printed device

Operational conditions

The optimization of operational conditions including stirring, dispensing rate, and injection volume was realized using a redox probe composed of 1 mmol L^{-1} $[Fe(CN)_6]^{4-/3-}$ prepared in 0.1 mol L^{-1} KCl. An aliquot of 40 mL of supporting electrolyte (0.1 mol L^{-1} KCl) was inserted into the BIA cell to realize the electrochemical experiments based on amperometry applying a detection potential of 0.25 V (vs CB/PLA). Electrochemical measurements in the absence and presence of stirring at 80 rpm were performed. The dispensing rate and injection volume were optimized in the range between 8.5–28 µL s^{-1} and 1–5 µL, respectively. Both parameters were studied keeping constant stirring at 80 rpm.

The stability of the p-RE was compared to a commercial RE composed of Ag/AgCl. For this purpose, electrochemical experiments were carried out using paracetamol (PAR) as a model analyte. Electrochemical experiments were realized in the presence of 1 mmol L^{-1} PAR prepared in two electrolytes composed of 0.1 mol L^{-1} Britton-Robinson buffer (pH 2 to 10) and KCl (0.01 to 2 mol L^{-1}). Cyclic voltammograms (CV) were recorded in the potential window between 0.0 and 1.2 V at a scan rate of 50 m Vs^{-1}.

Electrochemical measurements

The BIA cell with eight integrated electrodes was used for multiple electrochemical experiments. Freshly activated electrode (#1), GO/activated electrode (#2), and GOx/activated electrode (#3) were dedicated for electrochemical impedance spectroscopy (EIS) measurements (frequency range = 10^5 to 10^{-1} Hz, amplitude potential = 20 mV, and open-circuit potential = 0.23 V) in the presence of $[Fe(CN)_6]^{4-/3-}$ prepared in 0.1 mol L^{-1} KCl. The modification of integrated electrodes through GO and GOx was realized based on ex situ protocol adapted to recent studies [48, 49] (additional information is available in the ESI). These experiments were performed to estimate the electron transfer resistance (R_{ct}) value and heterogeneous electron transfer rate constant (Ks). In the same way, freshly activated electrodes labeled as #4, #5, #6, #7, and #8 were employed to evaluate the redox activities involving the biomolecule ADR. These experiments were performed through different electrochemical techniques including CV (window potential = − 1.0 to 1.0 V and scan rate = 0.05 V); linear sweep voltammetry (LSV) (window potential = 0.0 to 0.8 V and scan rate = 0.05 V); square wave voltammetry (SWV) (window potential = 0.0 to 0.5 V, frequency = 10 Hz, amplitude = 0.004 V, and potential increment = 0.002 V); differential pulse voltammetry (DPV) (window potential = 0.0 to 0.55 V, scan rate = 0.05 V s^{-1}, amplitude = 0.005 V, and modulation time = 30 ms), and amperometry (applied potential = 0.4 V vs Ag). Lastly, ADR was used as an analyte model to investigate the repeatability and reproducibility of the proposed 3D-printed BIA cell with integrated multiple electrodes. All voltammetric experiments were carried out applying the desirable potential vs p-RE.

Adrenaline analysis

The ADR analysis was performed through amperometric measurements applying a potential of 0.4 V (*vs* p-RE) to the working electrode (see Video S1). ADR standard solutions were prepared in 0.1 mol L^{-1} PBS (pH 7.2) containing 0.1 mol L^{-1} KCl [46]. To realize the recovery study, artificial urine samples were spiked with ADR standard solutions at three concentration levels (10, 20, and 30 µmol L^{-1}). For this experiment, solutions were prepared at a ratio of 1:1 (standard solution:artificial urine). The method used to prepare the artificial urine samples was adapted from a protocol described elsewhere [50]. All experiments were performed under optimized conditions.

Characterization

The fully 3D-printed sensing platform was characterized by scanning electron microscopy (SEM) using a microscope model JSM-6610 from JEOL (Akishima, Tokyo, Japan) via secondary electron imaging mode and acceleration voltage of 5 kV. The morphological study was realized by capturing images of WE surface, CB/PLA layers integrated into the wall from BIA, and interfaces between PLA, PLA-flex, and p-RE.

Results and discussion

Fabrication of the 3D-printed device

The use of 3D printing technology has been widely explored in the chemical sciences to manufacture analytical devices [51, 52]. Through a 3D printer equipped with single filaments, it is possible to create robust analytical systems, such as BIA [40]. Recently, the most modern BIA systems have advanced towards complete or partially 3D-printed electrode arrays. Richter and

Muñoz group, for example, have manufactured multiuse 3D-printed cells with single RE, AE, and WE based on the FDM method [40, 41]. As it is well-known, desktop printers equipped with multifilaments allow the simultaneous use of conductive, insulating, and flexible thermoplastic filaments, thus offering possibilities to create complete analytical devices with integrated sensing electrodes.

In this way, the current protocol proposes the printing of a 3D-printed BIA cell combined with multiple integrated electrodes. The 3D-printed cell is based on wall-jet configuration, and it can be rapidly mounted/dismounted by exploiting a threadable strategy, i.e., without sophisticated instrumentation. Overall, the proposed strategy makes the assembling rapid, practical, and simple. In addition, it opens real opportunities for allowing multiple routine analyses directly at the point of care. The sensing platform is composed of 5 printed segments, and it does not require other commercial components. Furthermore, it offers the possibility to print an entire BIA system with multiple integrated electrochemical cells. Each analytical platform was produced within 3.4 h at a cost of ~ U$ 1.2.

Morphological characterization

The morphological structure of the PLA, PLA-flex, CB/PLA, and silver ink painted over RE was evaluated through the SEM technique, as summarized in Figs. 2 and S4 (see ESI). As it can be seen in Fig. 2, the recorded SEM images show the entire circular area of WE (Fig. 2A), the layers of CB/PLA materials integrated on the 3D-printed cell wall (Fig. 2B), and the activated WE surface (Fig. 2C). The 3D-printed surface revealed well-defined edges and layers with low irregularity levels. The calculated diameter and layer thickness values for the WE were 3.55 ± 0.06 and 0.17 ± 0.02 mm, respectively. These mentioned values were compared to the theoretical dimensions (WE, $Ø = 3.5$ mm; thickness = 0.18 mm) and they demonstrated fidelity values from 90 to 98%.

Figure 2D and 2E depict SEM images detailing the interface between PLA and PLA-flex as well as the printed surface fully incorporated with Ag ink, respectively. As it can be noted in Fig. 2D, the printed surface has also presented a good edge definition and the morphology of the p-RE (Fig. 2E) was similar to the behavior reported in previous studies [41, 53].

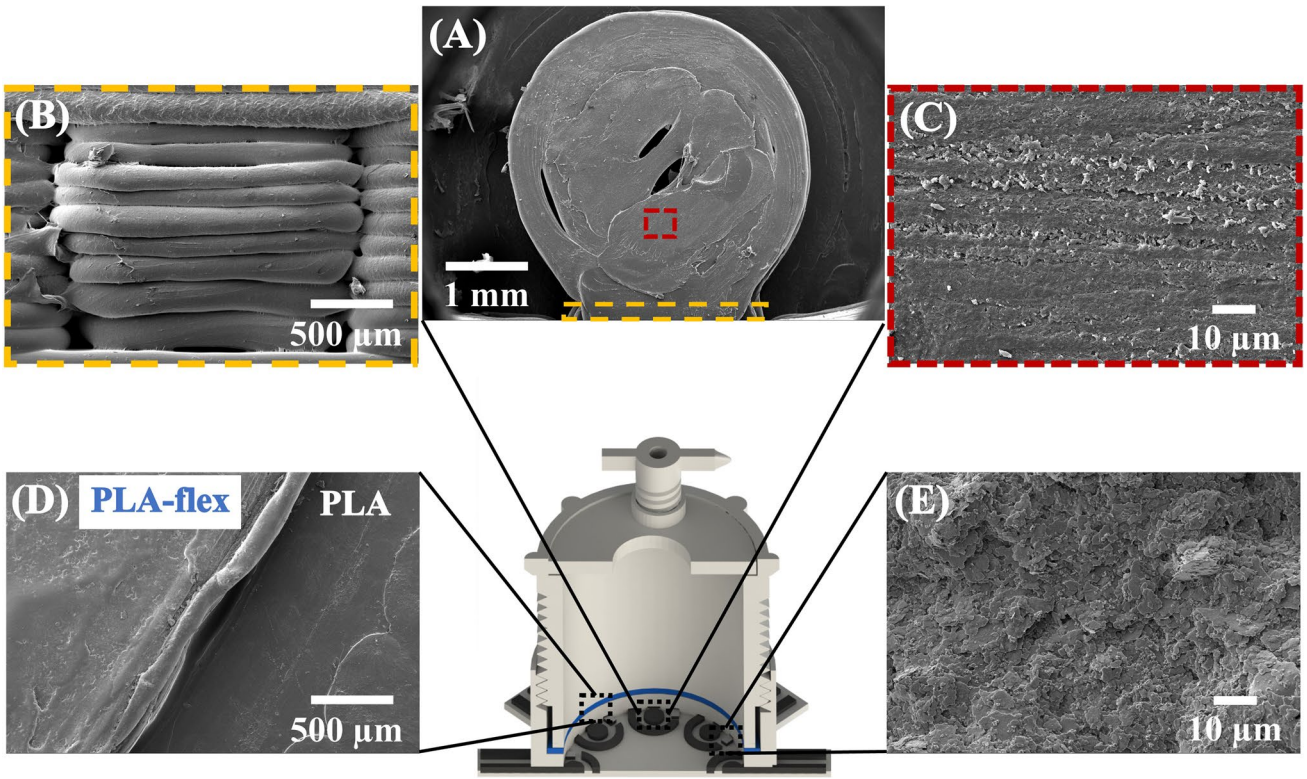

Fig. 2 SEM images showing **A** the geometric area of working electrode, **B** cross-section detailing the layer-by-layer deposition of electrode material and printed cell wall, **C** activated surface of working electrode, **D** interface between PLA/PLA-flex, and **E** surface of pseudo-reference electrode painted with Ag ink

Optimization of the 3D-printed cell operating conditions

It is well-known that the performance of BIA cell coupled to electrochemical detection depends on operational parameters including stirring, dispensing rate, and injection volume. For this reason, they were optimized to achieve the best performance. All experiments were realized using activated electrodes in the presence of $[Fe(CN)_6]^{4-/3-}$ prepared in 0.1 mol L^{-1} KCl as a redox mediator (Fig. 3). Additional information is summarized in Fig. S5 (see ESI).

Considering the achieved data (see additional discussion in the ESI), the best analytical performance was reached using stirring of 80 rpm, dispensing rate of 9 µL s^{-1}, and injection volume of 2 µL. Therefore, they were kept constant for the subsequent experiments.

Electrochemical performance of the integrated electrodes

The electrochemical performance of the integrated electrodes was evaluated using PAR solution as a model probe. These studies were performed in the presence of PAR prepared in BR buffer at pH values ranging from 2 to 10 and in KCl solution (0.01 to 2 mol L^{-1}). For this purpose, the performance of the printed sensor containing p-RE was compared to the data obtained using a commercial RE. The optimized data for peak potential and I_{pa} involving the PAR oxidation are shown in Figs. S6 and S7 (see in ESI). Based on the achieved data, it was possible to observe that both cells containing p-RE and commercial RE electrodes exhibited satisfactory peak potential responses with relative standard deviation (RSD) values ranging from 1.6 to 6.5%. Furthermore, considering the recorded values of I_{pa} associated to PAR oxidation in the presence of different KCl concentrations, it has been noticed that voltammetric response exploiting p-RE and commercial RE electrodes provided RSD values between 6.6 and 10.5%. Based on the achieved results, it can be noted that the 3D-printed BIA cell integrated with p-RE showed similar electrochemical performance when compared to commercial RE [53].

The 3D printing protocol based on FDM technology to construct BIA cell with integrated multiple electrodes offers affordable characteristics such as the printing of electrodes with different carbon-based filaments, also allowing their modification with different molecules depending on intended applications. Most importantly, the use of a BIA cell with multiple electrodes makes

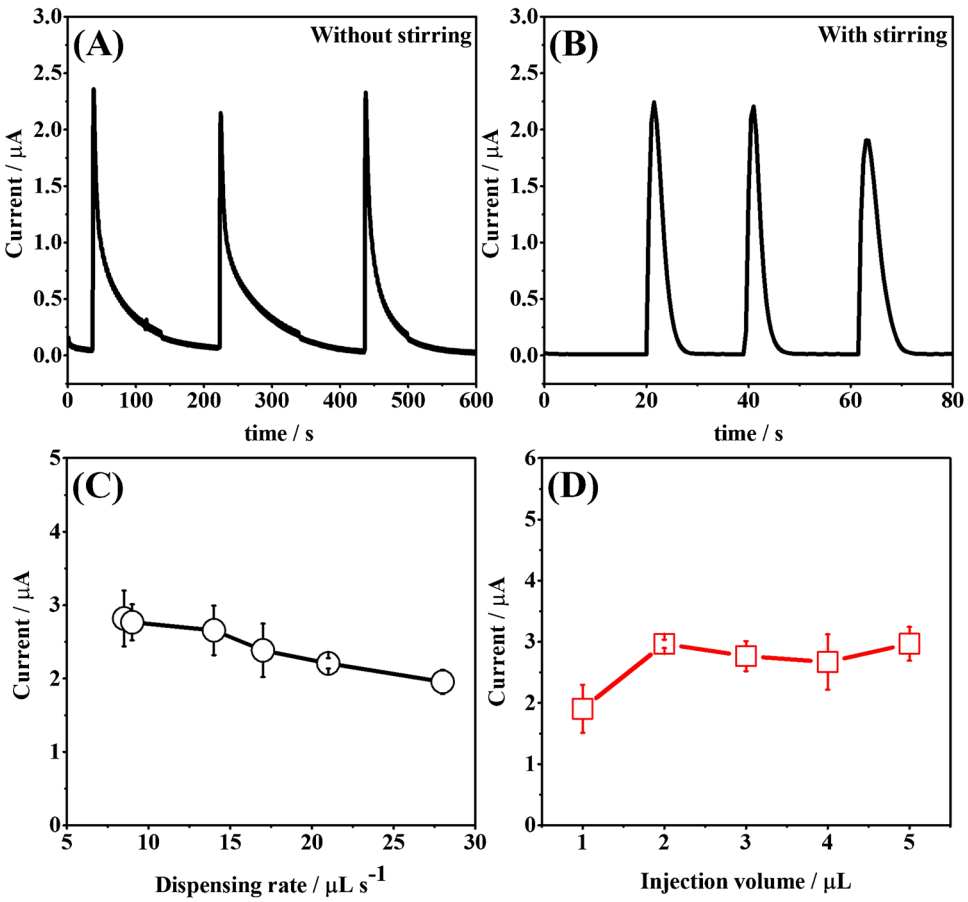

Fig. 3 Optimization of operational conditions of 3D printed BIA cell. Amperograms recorded for 1 mmol L^{-1} $[Fe(CN)_6]^{4-/3-}$ **A** without and **B** with stirring (80 rpm). Effect of **C** dispensing rate and **D** injection volume on the peak current. In **A**–**B**, the data were recorded using a dispensing rate of 9.0 µL s^{-1} and injection volume of 2.0 µL. In **C** and **D**, the injection volume and the dispensing rate were 2.0 µL and 9.0 µL s^{-1}, respectively. Supporting electrolyte: 0.1 mol L^{-1} KCl solution. All experiments were recorded applying 0.25 V *vs* CB/PLA

possible analytical applications with high-throughput or screening capabilities enabling, for example, sequential or multiplexed analyzes [49]. As proof of concept, the 3D-printed BIA cell with multiple integrated WE was evaluated through the modification with GO and GOx [48, 49] based on chitosan biofilm [48]. Furthermore, the redox activities of biomolecule ADR were carefully investigated by exploiting different electrochemical measurements involving CV, LSW, SWV, DPV, and AD. The summarized responses are denoted in Fig. 4.

As demonstrated in Fig. 4A, the activated printed surface in the absence (#1) and presence of GO (#2) and GOx (#3) presented distinct semicircle changes on Nyquist plots. The diagrams were fitted by a Randles circuit to estimate the electron transfer resistance (R_{ct}) values. The achieved R_{ct} values for electrodes #1, #2, and #3 were 1.4 ± 0.1, 3.5 ± 0.1, and 35 ± 2 kΩ ($n = 3$), respectively. Based on the achieved R_{ct} values and through Sluyters and Oomen methods [54, 55], the electron transfer rate constant (Ks) were estimated for each printed electrode and the calculated values for electrodes #1, #2, and #3 were $(1.5 \pm 0.1) \times 10^{-3}$, $(6.0 \pm 0.2) \times 10^{-4}$, and $(6.1 \pm 0.2) \times 10^{-5}$ cm s^{-1}, respectively.

As mentioned above, the R_{ct} and Ks values were drastically altered when the printed surfaces are incorporated with GO and GOx. This impedimetric behavior can be associated to impregnation of GO and GOx structures on electrode surface [56, 57]. It is important to mention that the GO/electrode and GOx/electrode are widely used in biological applications [58, 59]. As denoted in Fig. 4B using the electrode #4, the biomolecule ADR demonstrates well-defined peak potentials at 0.3 and − 0.2 V *vs* p-RE, indicating a quasi-reversible behavior (peak-to-peak separation ~ 500 mV). Following electrodes #5, #6, and #7 (Fig. 4C-E), it is possible to see the best redox activity for ADR at a potential range from 0.1 to 0.5 V *vs* p-RE. Next, the electrode #8 was used to optimize the ADR oxidation potential and the obtained responses are denoted in Fig. S8 (see in ESI).

Figure 4F exhibits the chronoamperograms showing the recorded response for the background current before and after the injection of a defined volume (2.0 µL) of 50 µmol

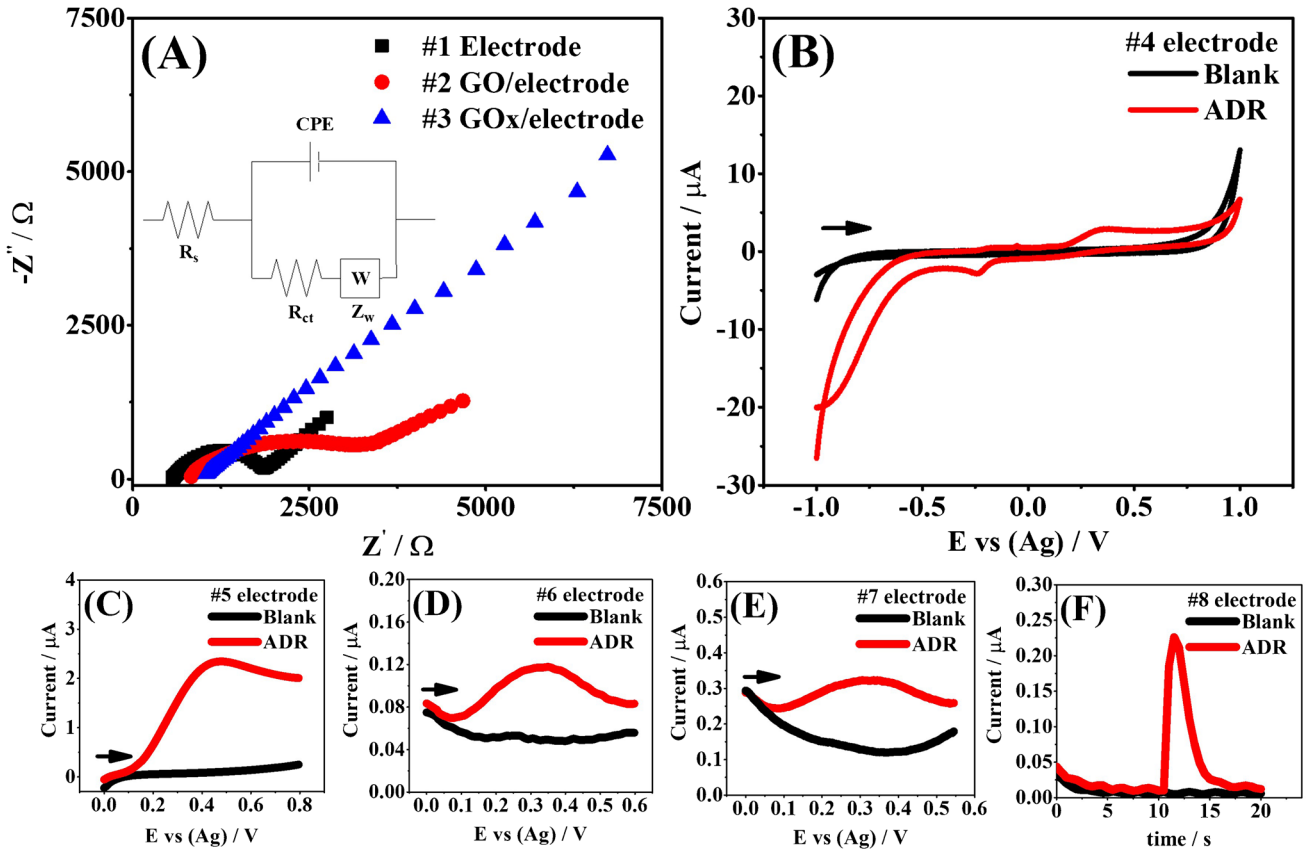

Fig. 4 Electrochemical characterization, study on redox activity, and amperogram recorded for ADR using eight integrated electrodes. **A** Nyquist plots recorded on electrodes #1, #2, and #3; **B**–**E** voltammograms recorded in the absence and presence of ADR through CV, LSV, SWV, and DPV techniques using electrodes #4, #5, #6, and #7, respectively; **F** typical amperogram showing the detection of ADR in the 3D-printed BIA-AD cell

L^{-1} ADR solution at optimized potential (0.4 V *vs* p-RE). These results indicated pronounceable faradaic performance with well-defined peaks involved in the oxidation of ADR catalyzed upon integrated 3D-printed electrode. It is important to mention that the optimized detection potential is similar to recent studies using carbon-based electrodes [60, 61].

Repeatability and reproducibility

Based on the optimized oxidation potential for ADR, the repeatability and reproducibility of the proposed 3D-printed BIA cell with eight integrated sensors were investigated by performing hydrodynamic experiments which were realized in inter- and intra-electrodes by successive injection of ADR solution (50 µmol L^{-1}). The obtained results are summarized in Fig. 5.

The RSD values calculated for experiments related to inter- ($n=8$) and intra-electrode ($n=3$) comparison ranged from 2 to 6%. The variance measurement through ANOVA-single factor was realized upon 3D-printed BIA cell responses exhibited in Fig. 5B (reproducibility study), and the obtained F value of 1.30 was lower than the F critical value (2.66), suggesting that the multiples integrated electrodes offer similar electrochemical responses, thus clearly highlighting the high-performance of the 3D-printed BIA cell with eight integrated electrodes for detection of ADR.

Analytical performance

As proof of concept, the 3D-printed analytical platform in association with amperometric detection (BIA-AD) was employed to measure ADR. The electrochemical oxidation of ADR was realized at 0.4 V *vs* p-RE, as previously mentioned in Fig. S8 (ESI). The analytical response and linear behavior of the electrochemical signal were investigated by ranging the ADR concentration between 5 and 40 µmol L^{-1} (Fig. 6).

The proposed BIA-AD system has exhibited an acceptable correlation coefficient ($R^2=0.99$) in the evaluated linear concentration range (5 to 40 µmol L^{-1}) and satisfactory limit of detection (LOD) for ADR (0.61 µmol L^{-1}). The LOD was calculated based on the 3S/slope of the analytical curve and it was compared to other reports found in the literature. As it can be seen in Table 1, the use of a 3D-printed electrochemical platform has offered a LOD value for ADR with magnitude order similar to those values found by bare electrodes. Based on the number of injections per hour, the analytical frequency (AF) was estimated to be ca. 494 ± 13 h^{-1}. The

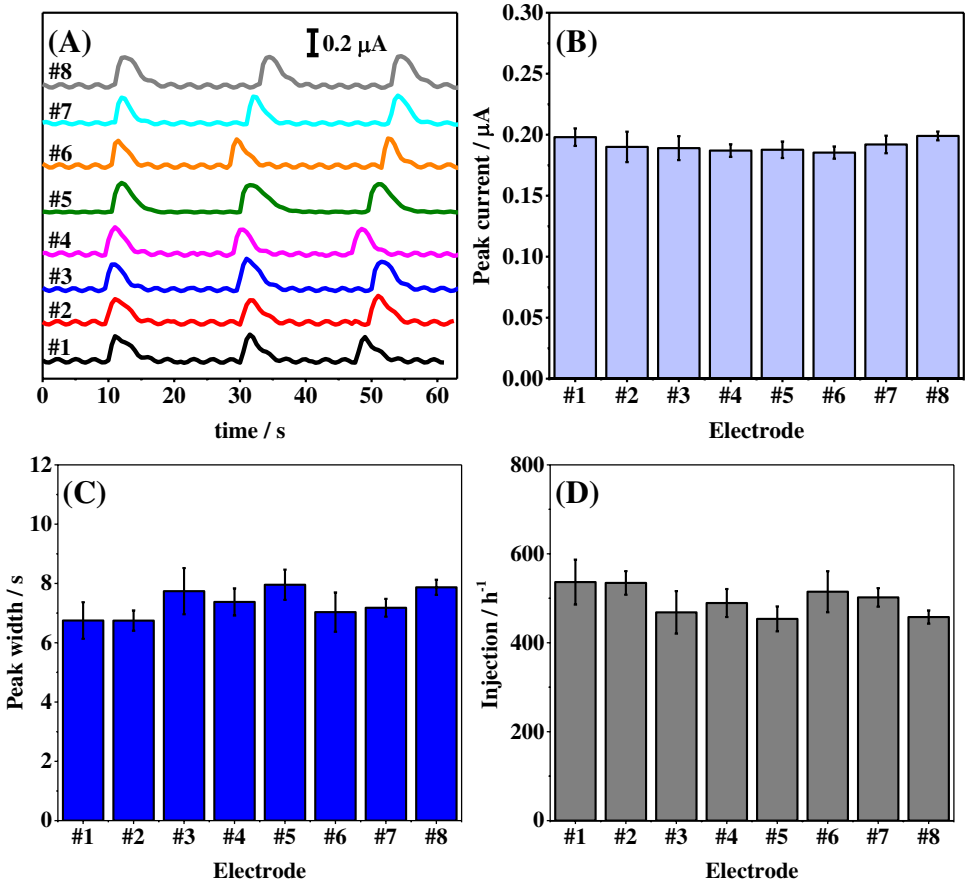

Fig. 5 Presentation of the electrochemical performance in terms of repeatability and reproducibility for ADR using 3D-printed electrodes. **A** Amperograms showing the detection of ADR at eight electrodes using the 3D-printed platform; graphs depicted in **B** and **C** show the peak current and width values for the results recorded at each electrode. Lastly, graph **D** displays the analytical sampling in terms of injection per hour for different electrodes. BIA conditions: injection volume = 2 µL; dispensing rate = 9.0 µL s^{-1}; stirring at 80 rpm. Model solution: 50 µmol L^{-1} ADR prepared in 0.1 mol L^{-1} PBS (pH = 7.2) and 0.1 mol L^{-1} KCl. All experiments were recorded applying 0.40 V *vs* p-RE

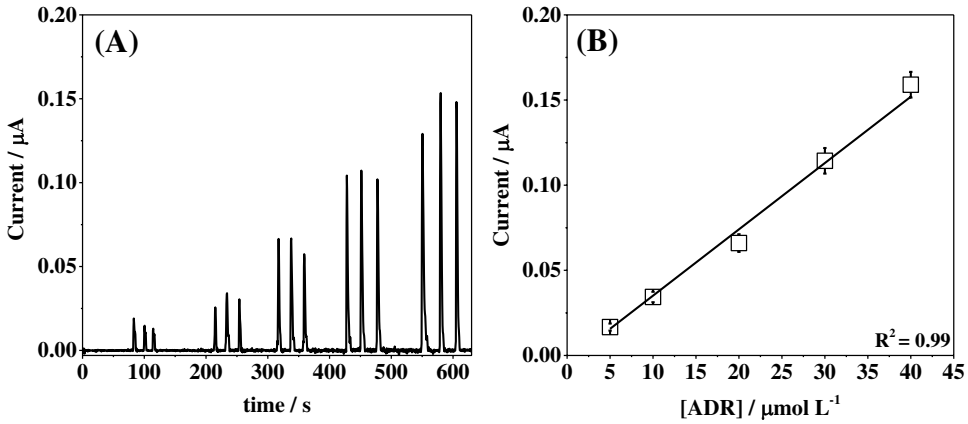

Fig. 6 **A** Amperogram showing the recorded response for ADR at different concentrations using BIA-AD system and **B** analytical curve demonstrating the linear dynamic concentration range ($y = -0.00383 + 0.00389x$). Experimental conditions: see Fig. 5

Table 1 Analytical features of the proposed analytical platform compared to the data reported by other electrochemical methods devoted to measurements of ADR

Electrode surface	Method	Linear range (µmol L^{-1})	LOD (µmol L^{-1})	Reference
MXene	AD	0.02–10	0.009	[46]
Stainless steel	AD	5–1000	1.0	[60]
NiO/CNT	SWV	0.08–900	0.01	[61]
BDD	SWV	0.7–60	0.21	[62]
GC	AD	NI	NI	[63]
Graphene	DPV	0.015–40	0.003	[64]
CQD	AD	0.02–0.8	0.006	[65]
$Ni_{3-x}Te_2$	SWV	4.0–31	0.35	[66]
Graphite	AD	100–2500	5.3	[67]
Au/GQD	AD	0.01–40	0.01	[68]
CB/PLA	AD	5–40	0.6	This study

BDD boron-doped diamond; *GC* glassy carbon; *CNT* carbon nanotube; *CQD* carbon quantum dot; *GQD* graphene quantum dot; *SWV* square wave voltammetry; *DPV* differential pulse voltammetry; *NI* no information.

AF value demonstrated herein is higher than other values reported using BIA systems constructed partially via 3D printing technology, as summarized in Table S1.

Aiming to demonstrate bioanalytical feasibility, the proposed BIA system was dedicated to realize measurements of ADR in artificial urine samples. This biological component is commonly used in asthma, defibrillation, cardiac arrest, and cardiopulmonary resuscitation cases [45, 46]. Furthermore, the coronavirus outbreak (COVID-19) has caused a significant demand for cardiopulmonary resuscitation drugs [69]. The recommended levels in human adult patients range from 0.5 to 1.0 mg kg^{-1} ADR [70]. For this reason, urine samples were spiked with ADR standard solutions in three concentration levels (10, 20, and 30 µmol L^{-1}). The recorded amperometric responses and a summary of the levels of ADR detected in the spiked samples are displayed in Fig. S9 (available in the ESI) and Table 2, respectively.

Table 2 Detected levels of ADR in artificial urine samples previously spiked with standard solutions at three concentration levels ($n = 3$

Spiking levels	Add (µmol L^{-1})	Found (µmol L^{-1})	Recovery (%)	RSD (%)
#1	10	11.9 ± 0.2	118 ± 1	2
#2	20	18.5 ± 0.3	92 ± 1	2
#3	30	25.9 ± 0.3	87 ± 1	1

The recovery study for ADR exhibited acceptable results in the range between 87 and 118%. It is important to note that the detection level of ADR evaluated herein is satisfactory for routine monitoring in clinical laboratories. Then, the proposed BIA-AD system indicated suitable analytical performance involving analysis of ADR in urine samples.

Conclusion

We have successfully demonstrated the use of a multimaterial open-source printer and distinct thermoplastic filaments to construct a fully 3D-printed BIA cell with multiple integrated sensing electrodes without commercial component requirements. The analytical system was manufactured using low-cost materials and its components can be quickly assembled/disassembled through a threadable strategy. The outstanding features of the 3D-printed BIA cell include the possibility of using multiple working electrodes potentially submitted to different surface modifications or sequential electrochemical measurements. Moreover, the integrated carbon black electrodes when associated with amperometric detection have provided a fast response for adrenaline measurements with adequate analytical performance. Based on the reported results, the 3D-printed BIA cell integrated

with sensing electrodes may emerge as a powerful and portable analytical tool for routine and high-throughput analysis.

Supplementary Information The online version contains supplementary material available at https://doi.org/10.1007/s00604-022-05323-4.

Acknowledgements The authors acknowledge the Multi-user Laboratory of high-resolution microscopy (LabMic/UFG) for using their facilities during SEM analysis.

Funding The authors received financial support and scholarships from CAPES (finance codes 88887.192880/2018-00 and 001), CNPq (grants 426496/2018–3, 308140/2016–8, 307554/2020–1, 142412/2020–1, and 405620/2021–7), and INCTBio (grant 465389/2014–7).

Declarations

Competing interests The authors declare no competing interests.

References

1. Ambrosi A, Pumera M (2016) 3D-printing technologies for electrochemical applications†. Chem Soc Rev 45:2740–2755. https://doi.org/10.1039/c5cs00714c
2. Chia HN, Wu BM (2015) Recent advances in 3D printing of biomaterials. J Biol Eng 9:1–14. https://doi.org/10.1186/s13036-015-0001-4
3. Gross B, Lockwood SY, Spence DM (2017) Recent advances in analytical chemistry by 3D printing. Anal Chem 89:57–70. https://doi.org/10.1021/acs.analchem.6b04344
4. Waheed S, Cabot JM, Macdonald NP et al (2016) 3D printed microfluidic devices: enablers and barriers. Lab Chip 16:1993–2013. https://doi.org/10.1039/c6lc00284f
5. O'Neil GD, Ahmed S, Halloran K et al (2019) Single-step fabrication of electrochemical flow cells utilizing multi-material 3D printing. Electrochem Commun 99:56–60. https://doi.org/10.1016/j.elecom.2018.12.006
6. Gross BC, Erkal JL, Lockwood SY, et al (2014) Evaluation of 3D printing and its potential impact on biotechnology and the chemical sciences. Anal Chem 86:3240–3253. https://doi.org/10.1021/ac403397r
7. Erkal JL, Selimovic A, Gross BC et al (2014) 3D printed microfluidic devices with integrated versatile and reusable electrodes. Lab Chip 14:2023–2032. https://doi.org/10.1039/c4lc00171k
8. Kadimisetty K, Malla S, Bhalerao KS et al (2018) Automated 3D-printed microfluidic array for rapid nanomaterial-enhanced detection of multiple proteins. Anal Chem 90:7569–7577. https://doi.org/10.1021/acs.analchem.8b01198
9. Glick CC, Srimongkol MT, Schwartz AJ et al (2016) Rapid assembly of multilayer micro fluidic structures via 3D-printed transfer molding and bonding. Microsyst Nanoeng 2:1–9. https://doi.org/10.1038/micronano.2016.63
10. Wei X, Li D, Jiang W et al (2015) 3D printable graphene composite. Sci Rep 5:1–7. https://doi.org/10.1038/srep11181
11. O'Neil GD (2020) Toward single-step production of functional electrochemical devices using 3D printing: progress, challenges, and opportunities. Curr Opin Electrochem 20:60–65. https://doi.org/10.1016/j.coelec.2020.02.023
12. Hamzah HH, Shafiee SA, Abdalla A, Patel BA (2018) 3D printable conductive materials for the fabrication of electrochemical sensors: a mini review. Electrochem Commun 96:27–31. https://doi.org/10.1016/j.elecom.2018.09.006
13. Carrasco-correa EJ, Simó-alfonso EF, Herrero-Martínez JM, Miró M (2021) The emerging role of 3D printing in the fabrication of detection systems. Trends Anal Chem 136:116177. https://doi.org/10.1016/j.trac.2020.116177
14. Carrasco-Correa EJ, Simó-Alfonso EF, Herrero-Martínez JM, Miró M (2021) The emerging role of 3D printing in the fabrication of detection systems. TrAC - Trends Anal Chem 136:116177. https://doi.org/10.1016/j.trac.2020.116177
15. Muñoz J, Pumera M (2020) 3D-printed biosensors for electrochemical and optical applications. TrAC - Trends Anal Chem 128:115933. https://doi.org/10.1016/j.trac.2020.115933
16. Yuk H, Lu B, Lin S et al (2020) 3D printing of conducting polymers. Nat Commun 11:1–8. https://doi.org/10.1038/s41467-020-15316-7
17. Cardoso RM, Kalinke C, Rocha RG et al (2020) Additive-manufactured (3D-printed) electrochemical sensors : a critical review. Anal Chim Acta 1118:73–91. https://doi.org/10.1016/j.aca.2020.03.028
18. Dias AA, Chagas CLS, Silva-Neto HA et al (2019) Environmentally friendly manufacturing of flexible graphite electrodes for a wearable device monitoring zinc in sweat. ACS Appl Mater Interfaces 11:39484–39492. https://doi.org/10.1021/acsami.9b12797
19. Kataoka ÉM, Murer RC, Santos JM et al (2017) Simple, expendable, 3D-printed microfluidic systems for sample preparation of petroleum. Anal Chem 89:3460–3467. https://doi.org/10.1021/acs.analchem.6b04413
20. Parra-Cabrera C, Achille C, Kuhn S, Ameloot R (2018) 3D printing in chemical engineering and catalytic technology: structured catalysts, mixers and reactors. Chem Soc Rev 47:209–230. https://doi.org/10.1039/c7cs00631d
21. Graham AD, Olof SN, Burke MJ, et al (2017) High-resolution patterned cellular constructs by droplet-based 3D printing. Sci Rep 7:1–11. https://doi.org/10.1038/s41598-017-06358-x
22. Duarte LC, Pereira I, Maciel LIL et al (2021) 3D printed microfluidic mixer for real-time monitoring of organic reactions by direct infusion mass spectrometry. Anal Chim Acta 1190:339252. https://doi.org/10.1016/j.aca.2021.339252
23. Beauchamp MJ, Nielsen Av, Gong H et al (2019) 3D printed microfluidic devices for microchip electrophoresis of preterm birth biomarkers. Anal Chem 91:7418–7425. https://doi.org/10.1021/acs.analchem.9b01395
24. Costa BMC, Coelho AG, Beauchamp MJ, et al (2022) 3D-printed microchip electrophoresis device containing spiral electrodes for integrated capacitively coupled contactless conductivity detection. Anal Bioanal Chem 414:545–550. https://doi.org/10.1007/s00216-021-03494-2
25. Chan HN, Shu Y, Xiong B et al (2016) Simple, cost-effective 3D printed microfluidic components for disposable, point-of-care colorimetric analysis. ACS Sensors 1:227–234. https://doi.org/10.1021/acssensors.5b00100
26. Li F, Macdonald NP, Guijt RM, Breadmore MC (2019) Increasing the functionalities of 3D printed microchemical devices by single material, multimaterial, and print-pause-print 3D printing. Lab Chip 19:35–49. https://doi.org/10.1039/c8lc00826d
27. Quintino MSM, Angnes L (2004) Batch injection analysis: an almost unexplored powerful tool. Electroanalysis 16:513–523. https://doi.org/10.1002/elan.200302878
28. Wang J (2002) Electrochemical detection for microscale analytical systems: a review. Talanta 56:223–231. https://doi.org/10.1016/S0039-9140(01)00592-6
29. Wang J, Taha Z (1991) Batch injection analysis. Anal Chem 63:1053–1056. https://doi.org/10.1021/ac00010a025

30. Almeida ES, Richter EM, Munoz RAA (2014) On-site fuel electroanalysis: determination of lead, copper and mercury in fuel bioethanol by anodic stripping voltammetry using screen-printed gold electrodes. Anal Chim Acta 837:38–43. https://doi.org/10.1016/j.aca.2014.05.031
31. Pereira PF, Marra MC, Munoz RAA, Richter EM (2012) Fast batch injection analysis system for on-site determination of ethanol in gasohol and fuel ethanol. Talanta 90:99–102. https://doi.org/10.1016/j.talanta.2012.01.004
32. Dias AA, Cardoso TMG, Cardoso RM et al (2016) Paper-based enzymatic reactors for batch injection analysis of glucose on 3D printed cell coupled with amperometric detection. Sens Actuators, B Chem 226:196–203. https://doi.org/10.1016/j.snb.2015.11.040
33. Tormin TF, Gimenes DT, Richter EM, Munoz RAA (2011) Fast and direct determination of butylated hydroxyanisole in biodiesel by batch injection analysis with amperometric detection. Talanta 85:1274–1278. https://doi.org/10.1016/j.talanta.2011.06.008
34. Stefano JS, Dias AC, Arantes IVS et al (2019) Batch-injection amperometric analysis on screen-printed electrodes: analytical system for high-throughput determination of pharmaceutical molecules. Electroanalysis 31:518–526. https://doi.org/10.1002/elan.201800725
35. Ferreira TP, de Sousa RA, Lowinsohn D (2016) Simultaneous determination of Pb and Cd in low-cost jewelry using differential pulse voltammetry. Anal Methods 8:8028–8032. https://doi.org/10.1039/C6AY02699K
36. Wang J, Taha Z (1991) Batch injection with potentiometric detection. Anal Chim Acta 252:215–221. https://doi.org/10.1016/0003-2670(91)87218-V
37. Rocha DP, Cardoso RM, Tormin TF et al (2018) Batch-injection analysis better than ever: new materials for improved electrochemical detection and on-site applications. Electroanalysis 30:1386–1399. https://doi.org/10.1002/elan.201800042
38. Tormin TF, Cunha RR, da Silva RAB et al (2014) Combination of screen-printed electrodes and batch injection analysis: a simple, robust, high-throughput, and portable electrochemical system. Sens Actuators, B Chem 202:93–98. https://doi.org/10.1016/j.snb.2014.04.096
39. Garcia PT, Dias AA, Souza JAC, Coltro WKT (2018) Batch injection analysis towards auxiliary diagnosis of periodontal diseases based on indirect amperometric detection of salivary α-amylase on a cupric oxide electrode. Anal Chim Acta 1041:50–57. https://doi.org/10.1016/j.aca.2018.08.039
40. Cardoso RM, Mendonça DMH, Silva WP et al (2018) 3D printing for electroanalysis: from multiuse electrochemical cells to sensors. Anal Chim Acta 1033:49–57. https://doi.org/10.1016/j.aca.2018.06.021
41. Richter EM, Rocha DP, Cardoso RM et al (2019) Complete additively manufactured (3D-printed) electrochemical sensing platform. Anal Chem 91:12844–12851. https://doi.org/10.1021/acs.analchem.9b02573
42. Palenzuela CLM, Novotny F, Krupička P, et al (2018) 3D-printed graphene/polylactic acid electrodes promise high sensitivity in electroanalysis. Anal Chem 90:5753–5757. https://doi.org/10.1021/acs.analchem.8b00083
43. Rocha DP, Squissato L, Silva SM et al (2020) Improved electrochemical detection of metals in biological samples using 3D-printed electrode : chemical / electrochemical treatment exposes carbon-black conductive sites. Electrochim Acta 335:1–11. https://doi.org/10.1016/j.electacta.2020.135688
44. Silva-Neto HA, Santhiago M, Duarte LC, Coltro WKT (2021) Fully 3D printing of carbon black-thermoplastic hybrid materials and fast activation for development of highly stable electrochemical sensors. Sens Actuators, B Chem 349:130721. https://doi.org/10.1016/j.snb.2021.130721
45. Brown HF, Difrancesco D, Noble SJ (1979) How does adrenaline accelerate the heart? Nature 280:235–236
46. Shankar SS, Shereema RM, Rakhi RB (2018) Electrochemical determination of adrenaline using MXene/graphite composite paste electrodes. ACS Appl Mater Interfaces 10:43343–43351. https://doi.org/10.1021/acsami.8b11741
47. Mclean-tooke APC, Bethune CA, Fay AC et al (2003) Adrenaline in the treatment of anaphylaxis : what is the evidence ? BMJ 327:8–11
48. Adumitrăchioaie A, Tertiș M, Suciu M et al (2019) A novel immunosensing platform for serotonin detection in complex real samples based on graphene oxide and chitosan. Electrochim Acta 311:50–61. https://doi.org/10.1016/j.electacta.2019.04.128
49. Fava EL, Silva TA, do Prado TM et al (2019) Electrochemical paper-based microfluidic device for high throughput multiplexed analysis. Talanta 203:280–286. https://doi.org/10.1016/j.talanta.2019.05.081
50. Sarigul N, Korkmaz F, Kurultak İ (2019) A new artificial urine protocol to better imitate human urine. Sci Rep 9:1–11. https://doi.org/10.1038/s41598-019-56693-4
51. Ligon SC, Liska R, Stampfl J, et al (2017) Polymers for 3D printing and customized additive manufacturing. Chem Rev 117:10212–10290. https://doi.org/10.1021/acs.chemrev.7b00074
52. Ngo TD, Kashani A, Imbalzano G et al (2018) Additive manufacturing (3D printing): a review of materials, methods, applications and challenges. Compos B Eng 143:172–196. https://doi.org/10.1016/j.compositesb.2018.02.012
53. Rohaizad N, Mayorga-Martinez CC, Novotný F et al (2019) 3D-printed Ag/AgCl pseudo-reference electrodes. Electrochem Commun 103:104–108. https://doi.org/10.1016/j.elecom.2019.05.010
54. Sluyters JH (1960) On the impedance of galvanic cells. Recueil 79:1092–1100. https://doi.org/10.1524/zpch.1967.52.1_4.089
55. Sluyters JH, Oomen JJC (1960) On the impedance of galvanic cells: II. Experimental verification. Recl Trav Chim Pays-Bas 79:1101–1110. https://doi.org/10.1002/recl.19600791014
56. Heterogeneous A, Transfer E (2020) Nitrogen-doped graphene : the influence of doping level on the charge-transfer resistance and apparent heterogeneous electron transfer rate. Sensors
57. Periasamy AP, Chang Y, Chen S (2011) Amperometric glucose sensor based on glucose oxidase immobilized on gelatin-multi-walled carbon nanotube modi fi ed glassy carbon electrode. Bioelectrochemistry 80:114–120. https://doi.org/10.1016/j.bioelechem.2010.06.009
58. Wilson R, Elizabeth Q (2016) Glucose oxidase : an ideal enzyme. Biosensors and Bioelectronic 5663:165–185
59. Wang Y, Li Z, Wang J et al (2011) Graphene and graphene oxide: biofunctionalization and applications in biotechnology. Trends Biotechnol 29:205–212. https://doi.org/10.1016/j.tibtech.2011.01.008
60. García-Miranda Ferrari A, Amor-Gutiérrez O, Costa-Rama E, Fernández-Abedul MT (2017) Batch injection electroanalysis with stainless-steel pins as electrodes in single and multiplexed configurations. Sens Actuators, B Chem 253:1207–1213. https://doi.org/10.1016/j.snb.2017.07.148
61. Gupta VK, Mahmoody H, Karimi F, et al (2017) Electrochemical determination of adrenaline using voltammetric sensor employing NiO/CNTs based carbon paste electrode. International J Electrochem Sci 12:248–257. https://doi.org/10.20964/2017.01.69
62. Sochr J, Švorc Ľ, Rievaj M, Bustin D (2014) Electrochemical determination of adrenaline in human urine using a boron-doped diamond film electrode. Diam Relat Mater 43:5–11. https://doi.org/10.1016/j.diamond.2014.01.005
63. Munshi AS, Martin RS (2016) Microchip-based electrochemical detection using a 3-D printed wall-jet electrode device. Analyst 141:862–869. https://doi.org/10.1039/c5an01956g

64. Zaidi SA (2018) Utilization of an environmentally-friendly monomer for an efficient and sustainable adrenaline imprinted electrochemical sensor using graphene. Electrochim Acta 274:370–377. https://doi.org/10.1016/j.electacta.2018.04.119
65. Shankar SS, Shereema RM, Ramachandran V et al (2019) Carbon quantum dot-modified carbon paste electrode-based sensor for selective and sensitive determination of adrenaline. ACS Omega 4:7903–7910. https://doi.org/10.1021/acsomega.9b00230
66. de Fatima Ulbrich K, Winiarski JP, Jost CL, Maduro de Campos CE (2020) Mechanochemical synthesis of a Ni3-xTe2 nanocrystalline composite and its application for simultaneous electrochemical detection of dopamine and adrenaline. Compos Part B: Eng 183:107649. https://doi.org/10.1016/j.compositesb.2019.107649
67. Agustini D, Fedalto L, Agustini D et al (2020) A low cost, versatile and chromatographic device for microfluidic amperometric analyses. Sens Actuators, B Chem 304:127117. https://doi.org/10.1016/j.snb.2019.127117
68. Vinoth V, Natarajan LN, Mangalaraja RV, et al (2019) Simultaneous electrochemical determination of dopamine and epinephrine using gold nanocrystals capped with graphene quantum dots in a silica network. Microchimica Acta 186:1–12. https://doi.org/10.1007/s00604-019-3779-9
69. Riphagen S, Gomez X, Gonzalez-Martinez C et al (2020) Hyperinflammatory shock in children during COVID-19 pandemic. The Lancet 395:1607–1608. https://doi.org/10.1016/S0140-6736(20)31094-1
70. Bateman ED, Hurd SS, Barnes PJ et al (2008) Global strategy for asthma management and prevention: GINA executive summary. Eur Respir J 31:143–178. https://doi.org/10.1183/09031936.00138707